Hindawi
Shock and Vibration
Volume 2019, Article ID 6743676, 10 pages
https://doi.org/10.1155/2019/6743676

Research Article

Snap-Through and Mechanical Strain Analysis of a MEMS Bistable Vibration Energy Harvester

Masoud Derakhshani and Thomas A. Berfield

Mechanical Engineering Department, University of Louisville, Louisville, KY 40292, USA

Correspondence should be addressed to Masoud Derakhshani; masoud.derakhshani@louisville.edu

Received 27 July 2018; Revised 17 October 2018; Accepted 30 January 2019; Published 4 March 2019

Academic Editor: Mohammad Rafiee

Vibration-based energy harvesting via microelectromechanical system- (MEMS-) scale devices presents numerous challenges due to difficulties in maximizing power output at low driving frequencies. This work investigates the performance of a uniquely designed microscale bistable vibration energy harvester featuring a central buckled beam coated with a piezoelectric layer. In this design, the central beam is pinned at its midpoint by using a torsional rod, which in turn is connected to two cantilever arms designed to induce bistable motion of the central buckled beam. The ability to induce switching between stable states is a critical strategy for boosting power output of MEMS. This study presents the formulation of a model to analyze the static and dynamic behaviors of the coupled structure, with a focus on the evolution of elongation strain within the piezoelectric layer. Cases of various initial buckling stress levels, driving frequencies, and driving amplitude were considered to identify regimes of viable energy harvesting. Results showed that bistable-state switching, or snap-through motion of the buckled beam, produced a significant increase in power production potential over a range of driving frequencies. These results indicate that optimal vibration scavenging requires an approach that balances the initial buckling stress level with the expected range of driving frequencies for a particular environment.

1. Introduction

Environmental concerns associated with conventional battery technologies coupled with a growing demand for small electronic sensors and devices make energy harvesting systems an intriguing power supply option for many applications. In cases where solar energy is not a viable alternative, vibration-based energy harvesting devices offer a comparable energy density solution provided that the application environment features a vibration source from which power can be scavenged.

One of the basic challenges for vibration energy harvesters is maximizing the power output of the system under what are typically chaotic, low-frequency vibration sources for real-life application environments. The lower range of operating frequencies (less than 200 Hz) is especially challenging for microscale energy harvesters due to natural frequency scaling inefficiencies as the feature dimensions shrink for MEMS-scale devices [1–3].

A number of works have concentrated on improving the operational frequency bandwidth and output power of MEMS-scale vibration energy harvesters, in particular through the use of nonlinear structures like buckled beams or plates. Betts et al. [4] studied both the static and dynamic response of uniquely arranged bistable composite plates with bonded piezoelectric patches functioning as a broadband vibration energy harvester. They found that while thicker laminate plates produce higher electrical energy when snap-through motion of the buckled plate occurred, the prevalence of such behavior was reduced due to the plate stiffness increase. The influence of bistable structure behavior in energy harvesting was further explored in several studies using an elastic support with an external magnet to induce bistable motion in the system at low-intensity vibrations [5, 6]. Additional works on variations of this design have focused on optimizing the active piezoelectric area in the system [7], utilizing the softening nonlinearities of the piezoelectric materials to lower the operating frequency [8], and investigating a vertical configuration of the cantilevered beam to work as an energy harvester [9]. Other studies have also examined the effects of buckled beam compression level

on dynamic behavior, as well as its influence on the transition between monostable and bistable responses [10–12] for simple structures.

Recent advances in the microfabrication processes have led to theoretical and experimental studies to enhance the efficiency of MEMS piezoelectric energy harvesters [13–15]. Ando et al. [16] presented a nonlinear vibration energy harvester based on the snap-through motion able to provide enough energy for an RF transmitter. The effects of nonlinearities on energy harvesting from a piezomagnetoelastic beam under random excitations were studied by De Paula et al. [17]. Both numerical and experimental results from that work showed the benefits of having snap-through motion in bistable structure systems compared to linear, monostable structures. The use of bistable thin-walled cylindrical shells [18] and thin plates with multiple piezoelectric layers [19] was also studied for optimized energy harvesting applications. Of direct significance to this work are additional studies that evaluated strain development in nonlinear clamped-clamped beams mounted with center proof masses [20] and an assessment of a buckled, asymmetric piezoelectric beam used as an energy harvesting system [21]. Both works demonstrated the benefits of frequency bandwidth expansion.

While there have been numerous studies on the performance analysis and improvement of the vibration energy harvesters, some unique challenges exist for the modeling and optimization of bistable structure systems under dynamic loading conditions. In this paper, the performance of a unique MEMS-scale bistable energy harvester designed to work at a moderately low-frequency range (below 200 Hz) is analytically investigated. This study extends a previous analysis [22] of a similar structure to enable prediction of power production under different behavior regimes for the microfabricated harvester. First, the theoretical formulation was developed for the dynamic behavior and mechanical elongation of the coupled structure. Then, using dimensions and material layers of a designed MEMS-scale device, a parametric analysis was performed to investigate the strain development within the piezoelectric layer as related to snap-through behavior of the buckled beam under different dynamic loading conditions. The results showed that the initial beam buckling stress and the base excitation amplitude are two major influences on the predicted vibration energy harvester performance.

2. Modeling Formulation

The structure considered in this work acts as a MEMS-scale vibration energy harvester that consists of a central, buckled beam with two stable buckled configurations. This design solves some of the difficulties presented by typical buckled structures used as vibration energy harvesters by generating snap-through motion at low frequencies more easily through the motion of coupled cantilever arms. The two cantilever arms with masses concentrated at their ends are connected to the central beam in a way making the 1st natural frequency easier to tailor to a particular vibration environment, separate from the dimensions and compressive stress state of the central beam. The large motion created in these arms is transferred to the main buckled beam through torsional rods, assisting the beam in switching between its stable states. The net result is that bistable motion can be readily facilitated over a range of driving frequency and amplitude combinations. Bistable motion in the central beam is particularly desirable as it produces large strains, boosting scavenged power output. This design is especially useful for MEMS-energy harvesters, which typically operate best at frequencies higher than most common real-life application environments (above 200 Hz) due to dimensional scaling laws.

Figure 1 shows a schematic model of the described MEMS-scale vibration energy harvester structure. A thin layer of piezoelectric material sandwiched by electrode metal layers covers the central beam to convert the induced mechanical strains into the electrical potential for power harvesting. The central beam is essentially pinned at its midpoint through connections to a torsional rod on each side. Parallel to the central beam, extending perpendicular from each torsional rod, are two cantilever arms with end tip masses. These attached cantilever arms serve the role of transferring vertical motion of the base to torques on the central buckled beam (inducing stable state switching), as well as improving the ability to reduce the first natural frequencies of the overall system. The entire structure is mounted on a moving base at four "clamped" support conditions where the central beam and torsional rod meet the base.

In this study, the electromechanical coupling effects of the piezoelectric layer are neglected in the structural modeling. In short, this assumes that the mechanical behavior of the composite structure is dominated by the material properties, regardless of the piezoelectric layer charge state. Justification for this assumption is that the stiffness/deformation response of the combined structure is generally unaffected by even the largest potential electrical charges the structure undergoes.

To simplify calculations, the stacked material layers were lumped into an equivalent cross-sectional area. Additional simplifications made include neglecting nonlinear effects of the torsional rod and cantilever arms, which preliminary experimental tests showed to be minimal. Thus, only nonlinearities in the central, buckled beam were considered. Based on these assumptions, nonlinear Euler–Bernoulli beam theory was used to express the equation of motion for each part of the system using Hamilton's principle:

$$\overline{m}_1 \frac{\partial^2 \widehat{W}_1}{\partial t^2} + EI_{y_1} \frac{\partial^4 \widehat{W}_1}{\partial x^4} + P \frac{\partial^2 \widehat{W}_1}{\partial x^2} + C_1 \frac{\partial \widehat{W}_1}{\partial t} - \frac{EA_1}{2L_1} \frac{\partial^2 \widehat{W}_1}{\partial x^2} \left[\int_0^{L_1} \left(\frac{\partial \widehat{W}_1}{\partial x} \right)^2 dx \right] = -\overline{m}_1 \frac{\partial^2 W_B}{\partial t^2}, \tag{1}$$

$$\rho J_p \frac{\partial^2 \phi}{\partial t^2} + C_2 \frac{\partial \phi}{\partial t} - G\gamma \frac{\partial^2 \phi}{\partial x^2} = 0, \tag{2}$$

$$\overline{m}_i \frac{\partial^2 \widehat{W}_i}{\partial t^2} + EI_{yi} \frac{\partial^4 \widehat{W}_i}{\partial x^4} + C_i \frac{\partial \widehat{W}_i}{\partial t} = -\overline{m}_i \frac{\partial^2 W_B}{\partial t^2}, \quad (i = 3, 4), \tag{3}$$

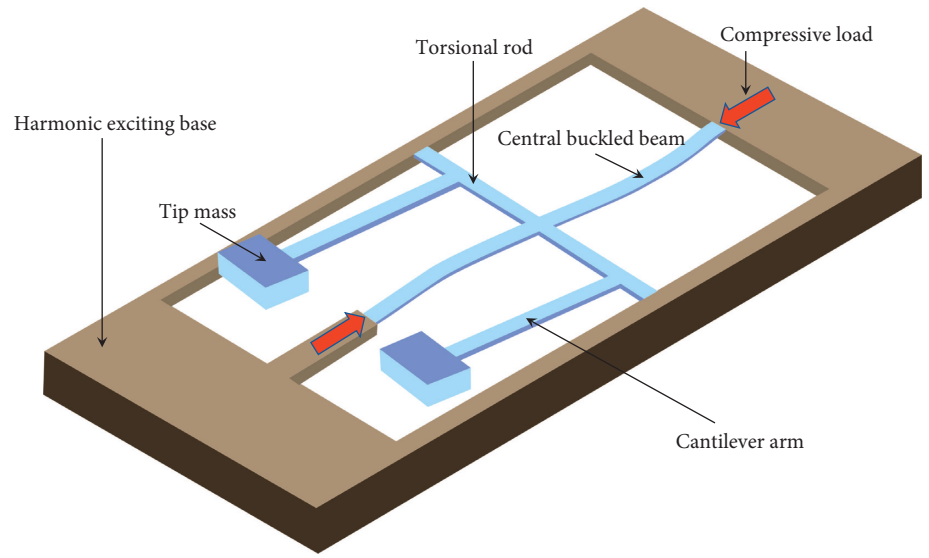

Figure 1: The schematic model of the buckled, bistable vibration energy harvester.

where $\widehat{W}_1$ is the lateral vibration of the main buckled beam, ϕ is the torsion of the middle rod, and $\widehat{W}_3$ and $\widehat{W}_4$ are the lateral vibrations of the cantilever arms. Parameters $\overline{m}, E, I, J, G, A, C, P,$ and W_B are mass per length, modulus of elasticity, second moment of area about the out of plane axis, polar second moment of area, shear modulus of elasticity, cross-sectional area, assumed damping coefficient, applied buckling load, and applied base vibration, respectively.

Since the proposed system consisted of different components, a component coupling method was required to accurately apply all the boundary and matching conditions at the connection points. To do so, the whole structure was divided into eight parts in total as shown in Figure 2. The above equations of motion were rewritten for each part based on the domains determined in Figure 2, resulting in eight equations in total rather than four. For simplicity, the subscriptions used in equations (1)–(3) were changed to $W_i\,(i = 1, 2, 7, 8)$ and $\phi_i\,(i = 3, 4, 5, 6)$ such that each number corresponded to that respective part of the system as labeled in Figure 2.

To find the response of the dynamic equation for each component of the system, the interactions between components must also satisfy the boundary conditions that exist at the connection points. To ensure this, the boundary conditions were derived as by-products from Hamilton's principle:

(i) Connection between the buckled beam and the torsional rod:

$$W_1'\left(\frac{l_1}{2}\right) = W_2'\left(\frac{l_1}{2}\right) = \phi_4\left(\frac{l_2}{2}\right) = \phi_5\left(\frac{l_2}{2}\right), \tag{4}$$

$$(EI)_1\left[W_1''\left(\frac{l_1}{2}\right) - W_2''\left(\frac{l_1}{2}\right)\right] + G\gamma\left[\phi_4'\left(\frac{l_2}{2}\right) - \phi_5'\left(\frac{l_2}{2}\right)\right] = 0. \tag{5}$$

(ii) Connection between the torsional rod and 1st cantilever arm:

$$\phi_3\left(\frac{l_2}{8}\right) = \phi_4\left(\frac{l_2}{8}\right) = W_7'(0), \tag{6}$$

$$(EI)_3 W_7''(0) + G\gamma\left[\phi_4'\left(\frac{l_2}{8}\right) - \phi_3'\left(\frac{l_2}{8}\right)\right] = 0. \tag{7}$$

(iii) Connection between the torsional rod and 2nd cantilever arm:

$$\phi_5\left(\frac{7l_2}{8}\right) = \phi_6\left(\frac{7l_2}{8}\right) = W_8'(0), \tag{8}$$

$$(EI)_3 W_8''(0) + G\gamma\left[\phi_6'\left(\frac{7l_2}{8}\right) - \phi_5'\left(\frac{7l_2}{8}\right)\right] = 0. \tag{9}$$

The total response of each component was then formed as a summation of static and dynamic responses as follows:

$$\begin{aligned} W_i(x,t) &= W_i^s(x) + V_i(x,t), \quad (i = 1, 2, 7, 8), \\ \phi_i(x,t) &= \phi_i^s(x) + f_i(x,t), \quad (i = 3, 4, 5, 6). \end{aligned} \tag{10}$$

For the static solution, the dynamic and damping parameters were dropped from equations (1)–(3). By doing so and applying the above matching conditions, a system of equations was developed, the general solution for which provides the exact static mode shapes and critical buckling loads of the system.

Galerkin's method then was used to discretize the dynamic equations of the system. This method required spatial functions around which the discretization process was performed. While the general condition required for these functions is satisfying the geometrical end boundaries of each component, finding exact shape functions of the linearized buckled system (which inherently meets all the geometrical and force-moment conditions at the

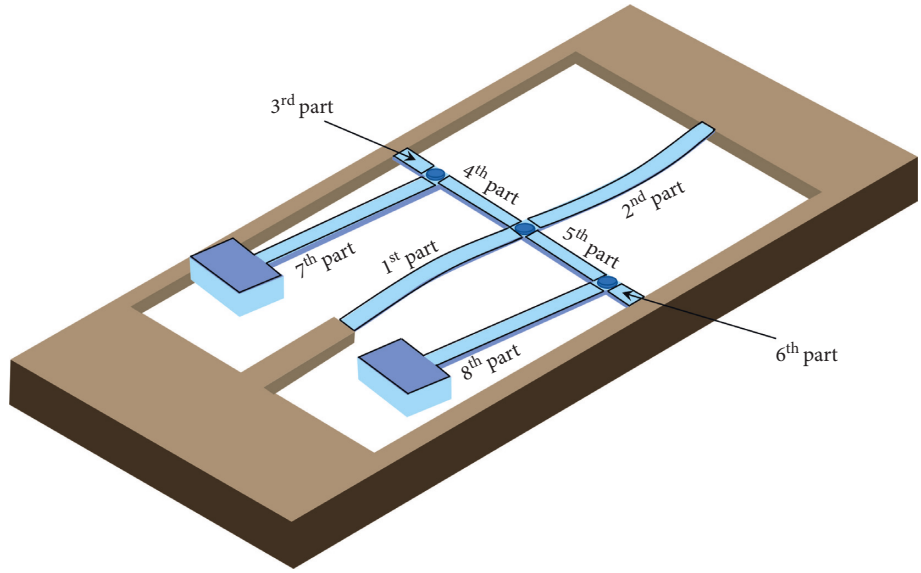

Figure 2: The coupled bistable structure divided into eight individual components.

connections) leads to a more accurate description of the nonlinear dynamic response. These general exact shape functions were derived from solving the undamped linearized dynamic equations, in which all the nonlinear, damping, and external force terms of equations (1)–(3) were set to zero. More details of the solving procedure and obtained shape functions for both static and dynamic parts may be found in [23].

By applying Galerkin's approach with the above linearized spatial shape functions, the following set of ordinary differential equations were obtained for all eight components of the energy harvesting system:

$$\sum_{j=1}^{N} m_{ij}^{n}\ddot{q}_{n}^{j} + \sum_{j=1}^{N} c_{ij}^{n}\dot{q}_{n}^{j} + \sum_{j=1}^{N} k_{ij}^{n}q_{n}^{j} + \sum_{j=1}^{N}\sum_{k=1}^{N} A_{ijk}^{n}q_{n}^{j}q_{n}^{k} + \sum_{j=1}^{N}\sum_{k=1}^{N}\sum_{l=1}^{N} B_{ijkl}^{n}q_{n}^{j}q_{n}^{k}q_{n}^{l} + f_{n}^{i} = 0, \quad (i = 1, 2, .., N), \ (n = 1, 2), \tag{11}$$

$$\sum_{j=1}^{N} m_{ij}^{n}\ddot{q}_{n}^{j} + \sum_{j=1}^{N} c_{ij}^{n}\dot{q}_{n}^{j} + \sum_{j=1}^{N} k_{ij}^{n}q_{n}^{j} = 0, \quad (i = 1, 2, \ldots, N), \ (n = 3 - 6), \tag{12}$$

$$\sum_{j=1}^{N} m_{ij}^{n}\ddot{q}_{n}^{j} + \sum_{j=1}^{N} c_{ij}^{n}\dot{q}_{n}^{j} + \sum_{j=1}^{N} k_{ij}^{n}q_{n}^{j} + f_{n}^{i} = 0, \quad (i = 1, 2, \ldots, N), \ (n = 7, 8), \tag{13}$$

where q_i^j is the i^{th} generalized coordinate of mode number j and $m_{ij}, c_{ij}, k_{ij}, A_{ijk}, B_{ijkl}$, and f^i are formed from the system shape functions and mechanical parameters. These discretized equations can be written in a matrix form for the total generalized coordinate vectors.

Equations (11)–(13) are uncoupled discretized equations for each part of the system. The matching conditions (4)–(9) must be satisfied not only for the spatial functions but also for the transient response. This requires a transformation from the total generalized coordinates to a new, independent set of generalized coordinates. As the strain response of the piezoelectric layer was of most importance to this study, the generalized coordinates of the first component (part 1) were considered as the independent coordinates in the transformation process. Applying geometrical matching conditions, i.e., equations (4), (6), and (8), produced the following relations between the first component and total generalized coordinates:

$$\underline{q} = [B]\underline{q}_1, \tag{14}$$

where $[B]$ is an $8N \times N$ transformation matrix and N is the number of considered modes in Galerkin's method. Inserting equation (14) into the discretized dynamic equations (11)–(13) followed by premultiplying by $[B]^{\mathrm{T}}$, the following reduced system of equations was obtained:

$$[M_{\mathrm{u}}]\ddot{\underline{q}}_1 + [C_{\mathrm{u}}]\dot{\underline{q}}_1 + [K_{\mathrm{u}}]\underline{q}_1 + \{\text{nonlinear vector}\}_{\mathrm{u}} = \underline{F}_{\mathrm{u}}, \tag{15}$$

where

$$\begin{aligned} [M_{\mathrm{u}}] &= [B]^{\mathrm{T}}[M][B], \\ [C_{\mathrm{u}}] &= [B]^{\mathrm{T}}[C][B], \\ [K_{\mathrm{u}}] &= [B]^{\mathrm{T}}[K][B], \\ \{\text{nonlinear vector}\}_{\mathrm{u}} &= [B]^{\mathrm{T}}\{\text{nonlinear vector}\}, \\ \underline{F}_{\mathrm{u}} &= [B]^{\mathrm{T}}\underline{F}. \end{aligned} \tag{16}$$

Solving equation (15) produced the nonlinear dynamic response of the central beam (part 1), which then was combined with the static part to build the total response of the main buckled beam for N considered modes. The resulting relation was formed as follows:

$$W_1(x,t) = W_1^s(x) + \sum_{i=1}^{N} \psi_1^i(x) q_1^i(t), \tag{17}$$

where $W_1^s(x)$ is the exact static function for a particular applied buckling load and $\psi_1^i(x)$ and $q_1^i(t)$ are the linearized shape functions and generalized coordinates of part 1 for mode i.

The response of the (31) plane was considered most critical for producing power from the piezoelectric layer, so analysis of the variation of the axial strain and elongation along the main buckled beam was essential for understanding the performance of this system as an effective vibration energy harvester. Based on the nonlinear Euler–Bernoulli beam theory, the axial strain relation for the buckled beam was written as follows:

$$\epsilon_{xx}(x,z,t) = \left[\frac{\partial U_1}{\partial x} + \frac{1}{2}\left(\frac{\partial W_1}{\partial x}\right)^2\right] - z\left(\frac{\partial^2 W_1}{\partial x^2}\right). \tag{18}$$

As shown in Figure 3, U_1 and W_1 are, respectively, the axial and lateral displacements of the first part of the nonlinear beam. As explained earlier here, analysis of the mechanical strain within the piezoelectric layer of the central beam gives an estimate of the power produced. Thus, the strain variation was calculated for the piezoelectric layer of the main beam at location $z = h_p$ as shown in Figure 3:

$$\epsilon_{xx}(x,t) = \left[\frac{\partial U_1}{\partial x} + \frac{1}{2}\left(\frac{\partial W_1}{\partial x}\right)^2\right] - h_p\left(\frac{\partial^2 W_1}{\partial x^2}\right). \tag{19}$$

Fixed-end "(clamped)" beam support conditions were assumed for the postbuckled configuration. For convenience, the entire length of the main beam was considered covered with the piezoelectric layer and electrodes. Therefore, the elongation of the piezoelectric layer of part 1 was formed as follows:

$$\Delta_1(t) = \frac{1}{2}\int_0^{l_1/2} \epsilon_{xx} dx = \frac{1}{2}\int_0^{l_1/2} \left(\frac{\partial W_1}{\partial x}\right)^2 dx - h_p \int_0^{l_1/2} \frac{\partial^2 W_1}{\partial x^2} dx. \tag{20}$$

Equation (20) indicated that the variation of the axial displacement of the main beam was contributed negligibly to the total elongation. Substituting equation (17) into the obtained elongation relation leads to the following equation:

$$\Delta_1(t) = \frac{1}{2}\int_0^{l_1/2} W_1^{s'2} dx - h_p \int_0^{l_1/2} W_1^{s''} dx + \sum_{i=1}^{N} \delta_1^i q_1^i(t) + \sum_{i=1}^{N}\sum_{j=1}^{N} \delta_2^{ij} q_1^i(t) q_1^j(t), \tag{21}$$

where

$$\delta_1^i = \int_0^{l_1/2} \left(W_1^{s'} \psi_1^{i'} - h_p \psi_1^{i''}\right) dx,\ \delta_1^{ij} = \frac{1}{2}\int_0^{l_1/2} \psi_1^{i'} \psi_1^{j'}\, dx, \quad (i, j = 1, 2, \ldots N). \tag{22}$$

where $\Delta_1(t)$ is the axial mechanical elongation of the first half of the main buckled beam. Similarly, the elongation for the second half of the beam (part 2) was developed as $\Delta_2(t)$, and finally, the whole beam elongation could be written as follows:

$$\Delta(t) = \Delta_1(t) + \Delta_2(t). \tag{23}$$

In order to estimate the potential output power of piezoelectric energy harvesters, the constitutive equations for a piezoelectric material were first considered [1]:

$$\begin{cases} D_z = d_{31}\sigma_{xx} + \epsilon_{33}^{\mathrm{T}} E_z, \\ \varepsilon_{xx} = d_{31} E_z + s_{11}^E \sigma_{xx}, \end{cases} \tag{24}$$

where $D_z, E_z, d_{31}, \epsilon_{33}$, and s_{11}^E were electrical displacement, electric field, permittivity, piezoelectric coupling coefficient, and elastic compliance of the stacked piezoelectric layer in the energy harvester device. By integrating equation (24) over the whole length of the piezoelectric layer, the predicted output charge and power of the bistable energy harvester assuming zero electric field and a purely resistive load were obtained as

$$Q(t) = \frac{b d_{31}}{s_{11}^E} \Delta(t), \tag{25}$$

$$P(t) = R\frac{dQ(t)}{dt}. \tag{26}$$

Results of the lateral displacement and mechanical elongation of a designed MEMS-scale device utilizing this model were explored in the next section for different harmonic driving excitations, applied buckling stresses, and excitation frequency levels. These cases were used to establish conditions corresponding to both snap-through and non-snap-through regimes. Furthermore, an estimation of the possible output power of the MEMS-energy harvester based on the developed model was performed. The results were then related to the effectiveness of power production for use as an energy harvester.

3. Results and Discussion

To model a realistic performance analysis of the bistable energy harvester, an actual designed MEMS-scale device was studied for various dimensional and initial condition parameters, as well as typical loading conditions. The experimental fabrication process of such a device was previously detailed in [24]. Figure 4 shows the top and side view of the analyzing device and dimensions, as well as the direction of the considered base excitation. In practice, MEMS-scale devices of this nature feature central beams with an initial buckling stress dictated by the microfabrication process parameters. Thus, this work provides dynamic behavior results organized by the initial buckling stress level, rather applied buckling force in the central beam.

An actual microscale energy harvester consists of different layers including structural, piezoelectric, and electrode layers. As explained in the previous section, this

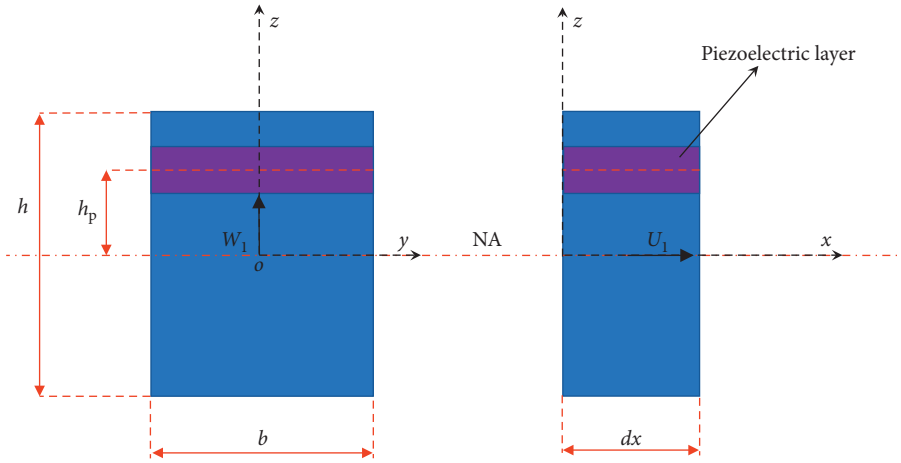

Figure 3: Schematic cross-sectional area and the distance of the piezoelectric layer from the neutral axis.

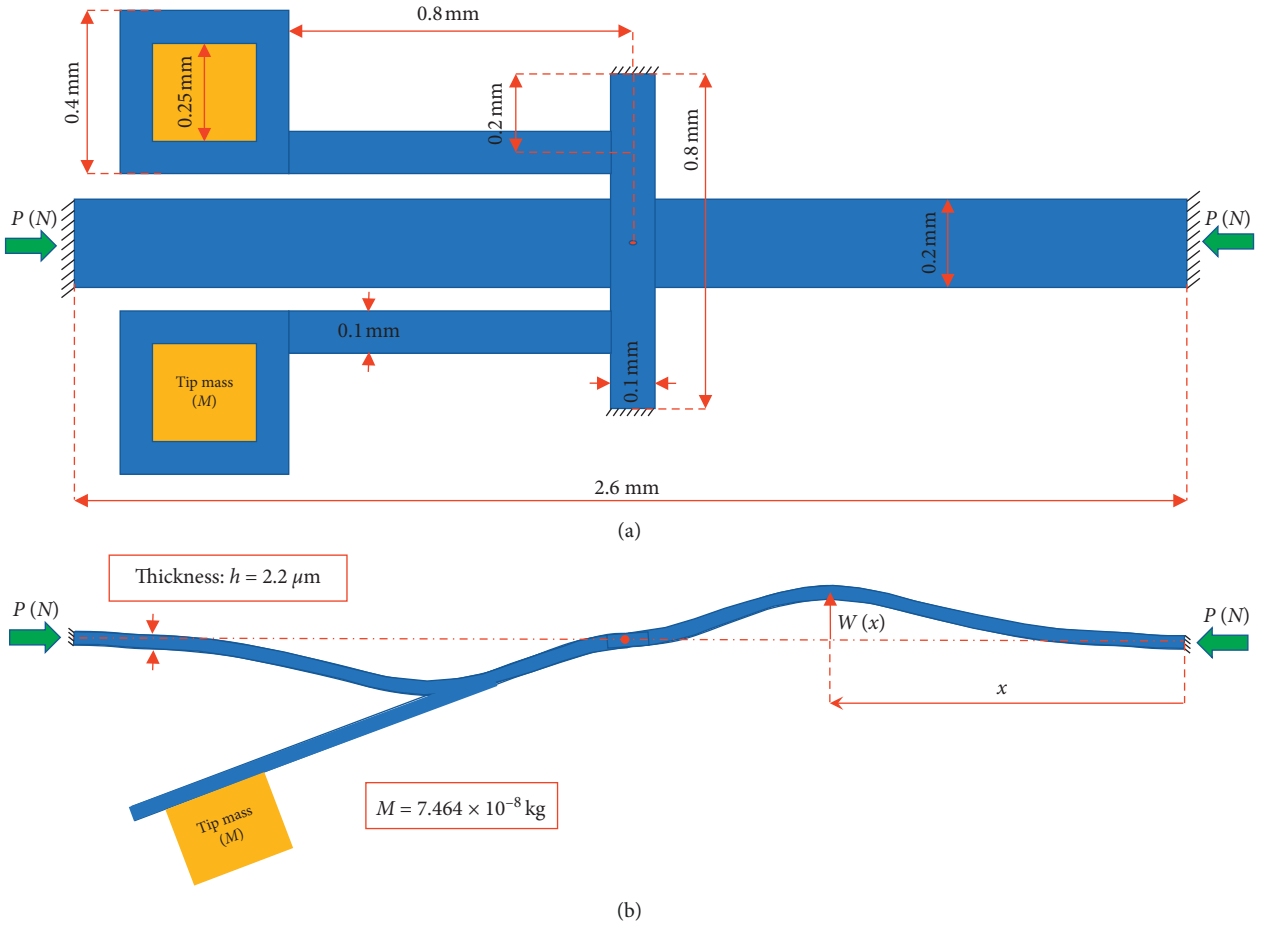

Figure 4: The designed MEMS-scale bistable energy harvester: (a) top view (b) side view.

formulation considers only the mechanical behavior of the materials included; that is, the electromechanical coupling components were neglected in the dynamic model. Figure 5 shows the schematic cross-sectional area of the proposed bistable energy harvester. The total height of the device and the thickness of each deposited layer are shown in the left side, while the equivalent cross-sectional area of a single modeled layer and its effective modulus of elasticity E, Poisson's ratio ν, and mass per length $\overline{m}$ are shown in the right side of the figure.

Solving the nonlinear static of the MEMS device gave the critical buckling loads (or critical buckling stress) and the static mode shapes of the system. The critical buckling stress obtained for the described system was 1.93 MPa, and its

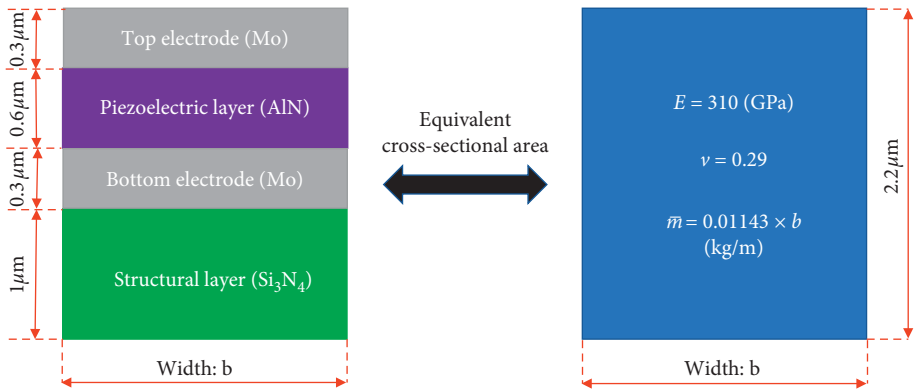

Figure 5: Different layers of the main buckled beam and its equivalent cross-sectional area parameters.

corresponding mode shape was found as shown in Figure 4(b). Moreover, natural frequencies and dynamic modes were found by solving the linearized dynamic equations provided in the modeling section, which required the given initial buckling stress induced in the structural layer. The first natural frequency of the designed MEMS-scale device with a 2 MPa buckling stress level, just above the obtained critical stress, was 115.6 Hz. This resonant frequency was relatively low for comparative microscale devices with similar overall size and geometry. Further results show that the first natural frequencies of the device do not change noticeably for higher considered buckling stress levels due to the fact that the system response was dominated by the dynamic behavior of the cantilever arms. The first five natural frequencies of the linearized buckled system are listed in Table 1.

Table 1: First five natural frequencies obtained for the MEMS-scale bistable energy harvester.

Mode shape	Mode 1	Mode 2	Mode 3	Mode 4	Mode 5
Natural frequencies (Hz)	115.6	7, 497.4	11, 381.6	13, 205.4	24, 711.1

Figure 6 shows a mapping of snap-through regimes of the studied MEMS-scale device for various base amplitudes versus the applied excitation frequency. The results were developed based on the presented modeling approach and assumption of a 1.94 MPa buckling stress, which was just above the critical stress required to produce a bistable system (an optimal configuration for inducing snap-through during vibration driving). The first three modes were considered for each part in the Galerkin discretization (equations (12)–(14)), and a harmonic driving motion was assumed for the base excitation. As shown in Figure 6, the base excitation required for the energy harvester to produce a bistable transition (snap-through motion) decreased with increasing excitation frequency until reaching its minimum at the system's first natural frequency. After passing the resonant frequency, the base excitation required to produce snap-through starts to increase for higher frequencies. This result indicates that snap-through motion and the associated higher power output is most feasible about a range of driving excitations near its first natural frequency, with larger base amplitudes enabling a greater range of snap-through producing excitation frequencies.

As the mechanical elongation of the piezoelectric layer in the main beam is directly related to the harvested output power, it is important to know how this elongation changes under various loading situations. Figure 7 shows the variation of the mechanical elongation amplitude of the device part 1 versus buckling stress while driven at an excitation frequency of 115 Hz. For each data point (compressive stress level) shown in Figure 7, the driving base excitation was set at the minimum level required for inducing snap-through behavior (ranged from 1 micron to 16 microns). As can be seen from the figure, the mechanical elongation rises with increased initial buckling stress. However, the rate of this improvement declines as the level of buckling increases due to the system getting stiffer.

Mechanical elongation amplitude of the piezoelectric layer in the main buckled beam was modeled for three different initial buckling stresses and a range of driving base excitation amplitudes applied at a frequency of 115 Hz (Figure 8). As shown for all three buckling levels, the elongation increases gradually when the system vibrates about one of its buckled states, i.e., the system demonstrates monostable motion within a single stable configuration. By increasing the base excitation above a critical level, there is a sudden jump in elongation amplitude for all three cases, which refers to the transition from monostable (local) motions to bistable (snap-through) motions. This illustrates how capturing snap-through can improve the harvested power output in the system. The point at which this rapid increase in the elongation occurs shifted with increased buckling stress level. After this abrupt transition, there are modest increases observed in the mechanical elongation for higher driving excitation amplitudes.

To estimate the output power harvested from the piezoelectric layer in the device, the piezoelectric coupling coefficient (d_{31}) of a fabricated aluminum nitride layer was assumed to be −3.5 pm/V from [25]. By inserting the aluminum nitride properties into equations (25) and (26), the zero electric field condition charge and harvested power of the MEMS-energy harvester for a purely resistive load were calculated from the model-predicted mechanical elongation of the piezoelectric layer. Two cases of buckling stress level $\sigma = 1.5\sigma_{cr}$ and $\sigma = 2\sigma_{cr}$ were considered for the output

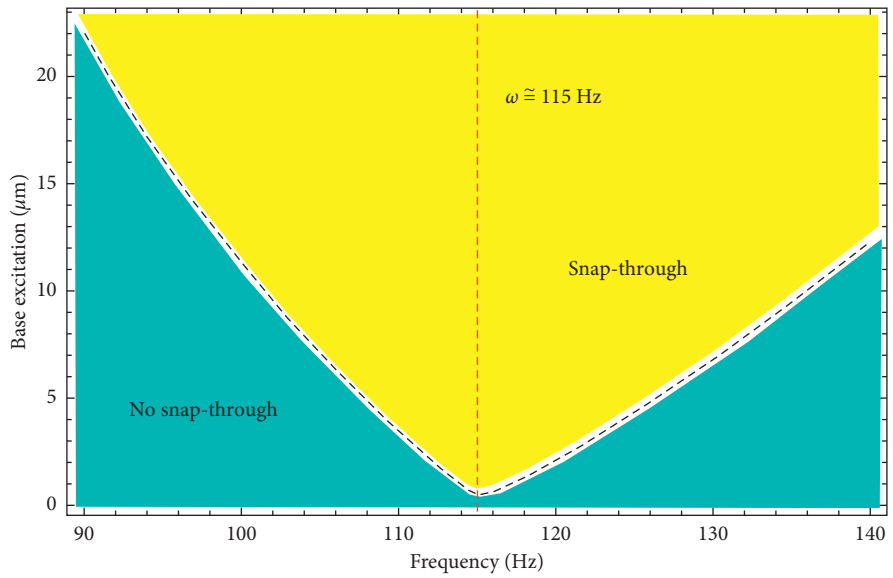

Figure 6: Variation of required base amplitude for the snap-through motion versus exciting frequency.

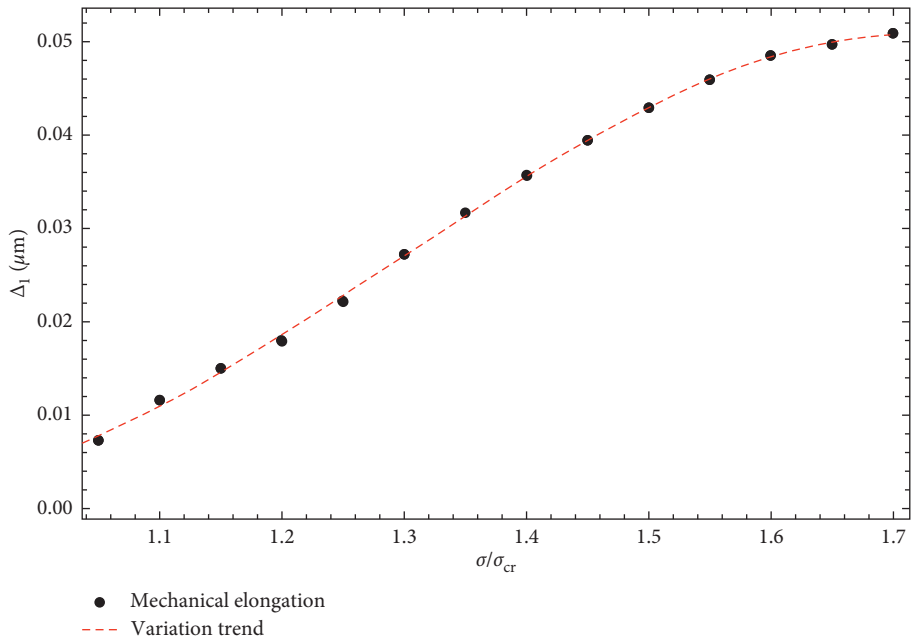

Figure 7: Variation of the main beam elongation amplitude versus central beam compressive stress level (normalized by the critical buckling stress) subjected to vibration source amplitudes corresponding to the minimum required for bistable motion at each stress level, applied at 115 Hz excitation frequency.

power estimation. The results showed that the maximum amplitude of the harvested power for 100 kΩ external resistive load and 115 Hz excitation frequency was in the range of 0.05 – 0.25 pW for 10 μm amplitude of base excitation which made the device have only local or monostable motion. However, this harvested power increased to 0.2 – 1 nW for 1 mm base amplitude (a more realistic condition for an actual device) in which snap-through and chaotic motions occurred. These results are provided to show the relative amount of harvested power produced by the two configurations of the system described in Figure 4. Improved power output could be gained through selection of materials and dimensional parameters optimized to a particular vibration source.

The last figure shows a regime plot of snap-through behavior for the microscale device for initial buckling stress versus driving excitation frequency (Figure 9). The results in Figure 9 were obtained for 20 μm amplitude of base excitation. As shown in the figure, the frequency bandwidth within which snap-through was predicted gets narrower as the buckling stress increases. Thus, the primary benefit of "just" buckled systems is the broadband performance as an energy harvester. However, the mechanical elongation and associated output power captured for these low initial

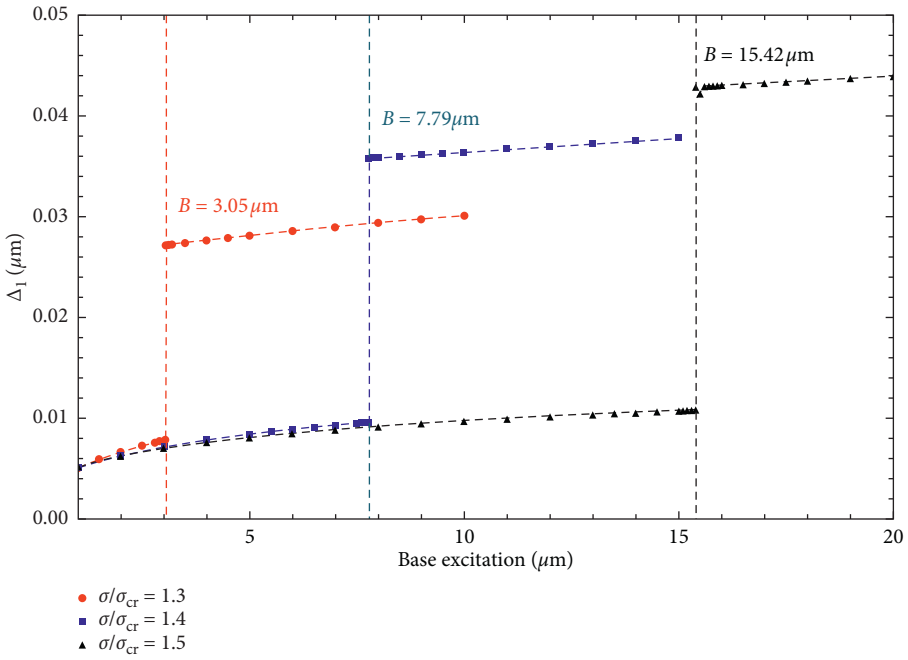

Figure 8: Variation of main beam elongation versus base excitation for three different initial buckling stress levels at 115 Hz excitation frequency.

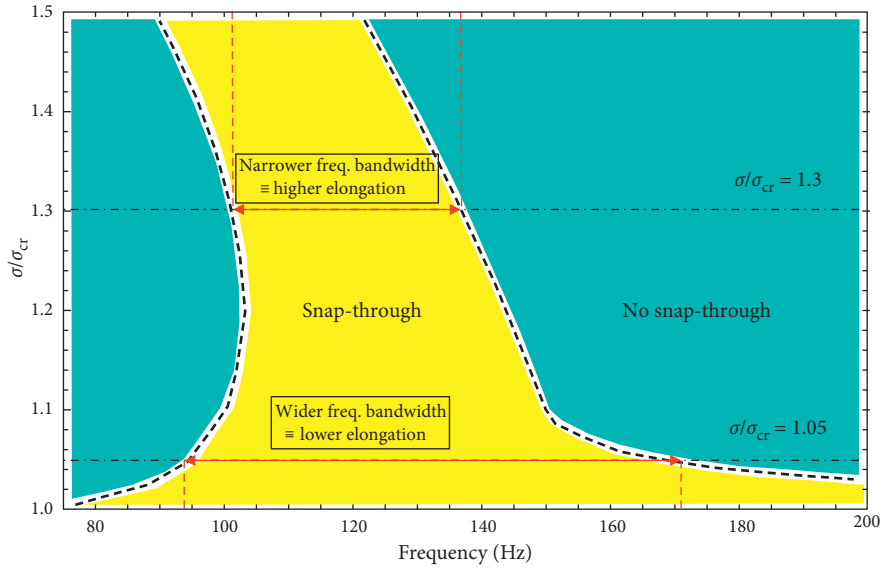

Figure 9: Snap-through regime plot of the MEMS device for buckling stress versus exciting frequency.

buckling stress cases are outperformed by higher initial buckled cases, provided that the driving excitation amplitude is sufficient to induce bistable motion. These results indicate optimum energy harvesting power output for this bistable device requires a need to tailor the initial buckling stress parameter within the fabricated layers to both the operating frequency bandwidth and the driving amplitude.

4. Conclusion

The dynamic model of the microscale bistable energy harvester developed in this study showed that initiation of snap-through switching of the central buckled beam creates a dramatic increase in the strain elongation of the piezoelectric layer and consequently the harvested power of the device. It was also found that central beams with initial buckling stress just above the critical level produce devices with the broader band of operating frequencies viable for power production. Further strain potential and harvested power could be gained with even larger initial buckling stress levels, though at a sacrifice to operation frequency range, provided that sufficient driving amplitude must be supplied to induce snap-through motion. Optimal vibration energy scavenging capability requires balancing the

trade-off between these factors associated with the targeted vibration source.

Data Availability

No external datasets were used to support this study.

Conflicts of Interest

The authors declare that there are no conflicts of interest regarding the publication of this paper.

Acknowledgments

This research was funded by the National Science Foundation, via Award #1408005 within Electrical, Communication, and Cyber System (ECCS) Division.

References

[1] A. Erturk and D. J. Inman, *Piezoelectric Energy Harvesting*, John Wiley & Sons, Hoboken, NJ, USA, 2011.

[2] H. S. Kim, J.-H. Kim, and J. Kim, "A review of piezoelectric energy harvesting based on vibration," *International Journal of Precision Engineering and Manufacturing*, vol. 12, no. 6, pp. 1129–1141, 2011.

[3] R. L. H. a. K. Wang, "A review of the recent research on vibration energy harvesting via bistable systems," *Smart Materials and Structures*, vol. 22, no. 2, article 023001, 2013.

[4] D. Betts, H. Kim, C. Bowen, and D. Inman, "Static and dynamic analysis of bistable piezoelectric-composite plates for energy harvesting," in *Proceedings of 53rd AIAA/ASME/ASCE/AHS/ASC Structures, Structural Dynamics and Materials Conference 20th AIAA/ASME/AHS Adaptive Structures Conference 14th AIAA*, Honolulu, HI, USA, April 2012.

[5] Y. Gao, Y. G. Leng, S. B. Fan, and Z. H. Lai, "Performance of bistable piezoelectric cantilever vibration energy harvesters with an elastic support external magnet," *Smart Materials and Structures*, vol. 23, no. 9, article 095003, 2014.

[6] Y. Leng, Y. J. Gao, D. Tan, S. B. Fan, and Z. H. Lai, "An elastic-support model for enhanced bistable piezoelectric energy harvesting from random vibrations," *Journal of Applied Physics*, vol. 117, no. 6, article 064901, 2015.

[7] S. Du, Y. Jia, and A. Seshia, "Maximizing output power in a cantilevered piezoelectric vibration energy harvester by electrode design," *Journal of Physics: Conference Series*, vol. 60, article 012114, 2015.

[8] S. Leadenham and A. Erturk, "Unified nonlinear electroelastic dynamics of a bimorph piezoelectric cantilever for energy harvesting, sensing, and actuation," *Nonlinear Dynamics*, vol. 79, no. 3, pp. 1727–1743, 2015.

[9] S. F. A. Michael I Friswell, O. Bilgen, S. Adhikari, A. W. Lees, and G. Litak, "Non-linear piezoelectric vibration energy harvesting from a vertical cantilever beam with tip mass," *Journal of Intelligent Material Systems and Structures*, vol. 23, no. 13, pp. 1505–1521, 2012.

[10] J. Qiu, J. H. Lang, and A. H. Slocum, "A curved-beam bistable mechanism," *Journal of Microelectromechanical Systems*, vol. 13, no. 2, pp. 137–146, 2004.

[11] J. Casals-Terre, A. Fargas-Marques, and A. M. Shkel, "Snap-action bistable micromechanisms actuated by nonlinear resonance," *Journal of Microelectromechanical Systems*, vol. 17, no. 5, pp. 1082–1093, 2008.

[12] F. Cottone et al., "Piezoelectric buckled beams for random vibration energy harvesting," *Smart Materials and Structures*, vol. 21, no. 3, article 035021, 2012.

[13] Ö. Zorlu and H. Külah, "A MEMS-based energy harvester for generating energy from non-resonant environmental vibrations," *Sensors and Actuators A: Physical*, vol. 202, pp. 124–134, 2013.

[14] M. Rezaeisaray, M. EI Gowini, D. Sameoto, D. Raboud, and W. Moussa, "Low frequency piezoelectric energy harvesting at multi vibration mode shapes," *Sensors and Actuators A: Physical*, vol. 228, pp. 104–111, 2015.

[15] R. Xu and S. Kim, "Low-frequency, low-G MEMS piezoelectric energy harvester," *Journal of Physics: Conference Series*, vol. 660, article 012013, 2015.

[16] B. Andò, S. Baglio, A. R. Bulsara, V. Marletta, and A. Pistorio, "Experimental and theoretical investigation of a nonlinear vibrational energy harvester," *Procedia Engineering*, vol. 120, pp. 1024–1027, 2015.

[17] A. S. De Paula, D. J. Inman, and M. A. Savi, "Energy harvesting in a nonlinear piezomagnetoelastic beam subjected to random excitation," *Mechanical Systems and Signal Processing*, vol. 54–55, pp. 405–416, 2015.

[18] Y. Wang, L. Peng, and Z. Huang, "Structural optimum design of bistable cylindrical shell for broadband energy harvesting application," *Theoretical and Applied Mechanics Letters*, vol. 5, no. 4, pp. 151–154, 2015.

[19] U. Aridogan, I. Basdogan, and A. Erturk, "Random vibration energy harvesting on thin plates using multiple piezopatches," *Journal of Intelligent Material Systems and Structures*, vol. 27, no. 20, pp. 2744–2756, 2016.

[20] A. Emad, M. A. E. Mahmoud, M. Ghoneima, and M. Dessouky, "Testing and evaluation of stretching strain in clamped–clamped beams for energy harvesting," *Smart Materials and Structures*, vol. 25, no. 11, article 115006, 2016.

[21] L. Van Blarigan and J. Moehlis, "Dynamic analysis of a buckled asymmetric piezoelectric beam for energy harvesting," *Chaos: An Interdisciplinary Journal of Nonlinear Science*, vol. 26, no. 3, article 033107, 2016.

[22] M. Derakhshani, T. Berfield, and K. D. Murphy, "Dynamic analysis of a Bi-stable buckled structure for vibration energy harvester," *Dynamic Behavior of Materials*, Springer, vol. 1, , pp. 199–208, 2018.

[23] M. Derakhshani, *Dynamic Analysis and Fabrication of a Bistable Structure Designed for MEMS Energy Harvesting Application*, University of Louisville, Louisville, KY, USA, 2019.

[24] M. Derakhshani, B. E. Allgeier, and T. A. Berfield, "Study on the fabrication process of a MEMS bistable energy harvester based on coupled component structures," *Mechanics of Biological Systems & Micro-and Nanomechanics*, vol. 4, pp. 75–79, 2019.

[25] E. Yarar, V. Hrkac, C. Zamponi, A. Piorra, L. Kienle, and E. Quandt, "Low temperature aluminum nitride thin films for sensory applications," *AIP Advances*, vol. 6, no. 7, article 075115, 2016.